Preservation of NOM-metal complexes in a modern hyperalkaline stalagmite: Implications for speleothem trace element geochemistry

Hartland, Adam; Fairchild, Ian J.; Müller, Wolfgang; Dominguez-villar, David

DOI:
10.1016/j.gca.2013.12.005

Available online at www.sciencedirect.com

ScienceDirect

Geochimica et Cosmochimica Acta 128 (2014) 29–43

Geochimica et Cosmochimica Acta

www.elsevier.com/locate/gca

Preservation of NOM-metal complexes in a modern hyperalkaline stalagmite: Implications for speleothem trace element geochemistry

Adam Hartland [a,*], Ian J. Fairchild [b], Wolfgang Müller [c], David Dominguez-Villar [d]

[a] Chemistry Department and Environmental Research Institute, Faculty of Science and Engineering, University of Waikato, Hamilton, New Zealand

[b] School of Geography, Earth and Environmental Sciences, University of Birmingham, Birmingham B15 2TT, UK

[c] Department of Earth Sciences, Royal Holloway University of London, Egham Hill, Egham, Surrey TW20 0EX, UK

[d] Centro Nacional de Investigación sobre la Evolución Humana, Paseo Sierra de Atapuerca S/n 09002, Burgos, Spain

Received 22 April 2013; accepted in revised form 4 December 2013; available online 14 December 2013

Abstract

We report the first quantitative study of the capture of colloidal natural organic matter (NOM) and NOM-complexed trace metals (V, Co, Cu, Ni) in speleothems. This study combines published NOM–metal dripwater speciation measurements with high-resolution laser ablation ICPMS (LA-ICPMS) and sub-annual stable isotope ratio ($\delta^{18}O$ and $\delta^{13}C$), fluorescence and total organic carbon (TOC) analyses of a fast-growing hyperalkaline stalagmite (pH ~11) from Poole's Cavern, Derbyshire UK, which formed between 1997 and 2008 AD. We suggest that the findings reported here elucidate trace element variations arising from colloidal transport and calcite precipitation rate changes observed in multiple, natural speleothems deposited at ca. pH 7–8. We find that NOM–metal$_{(aq)}$ complexes on the boundary between colloidal and dissolved (~1 nm diameter) show an annual cyclicity which is inversely correlated with the alkaline earth metals and is explained by calcite precipitation rate changes (as recorded by kinetically-fractionated stable isotopes). This relates to the strength of the NOM–metal complexation reaction, resulting in very strongly bound metals (Co in this system) essentially recording NOM co-precipitation (ternary complexation). More specifically, empirical partition coefficient (K_d) values between surface-reactive metals (V, Co, Cu, Ni) [expressed as ratio of trace element to Ca ratios in calcite and in solution] arise from variations in the 'free' fraction of total metal in aqueous solution (f_m). Hence, differences in the preservation of each metal in calcite can be explained quantitatively by their complexation behaviour with aqueous NOM. Differences between inorganic K_d values and field measurements for metal partitioning into calcite occur where [free metal] $\ll$ [total metal] due to complexation reactions between metals and organic ligands (and potentially inorganic colloids). It follows that where $f_m \approx 0$, apparent inorganic $K_{d\ app}$ values are also $\approx$0, but the true partition coefficient ($K_{d\ actual}$) is significantly higher. Importantly, the K_d of NOM–metal complexes [organic carbon–metal ratio) approaches 1 for the most stable aqueous complexes, as is shown here for Co, but has values of 24–150 for V, Ni and Cu. This implies that ternary surface complexation (metal–ligand co-adsorption) can occur (as for NOM–Co), but is the exception rather than the rule. We also demonstrate the potential for trace metals to record information on NOM composition as expressed through changing NOM–metal complexation patterns in dripwaters. Therefore, a suite of trace metals in stalagmites show variations clearly attributable to changes in organic ligand concentration and composition, and which potentially reflect the state of overlying surface ecosystems.

* Corresponding author. Tel.: +64 7 838 4466x8527; fax: +61 7 838 4219.
E-mail address: a.hartland@waikato.ac.nz (A. Hartland).

0016-7037/$ - see front matter © 2013 Elsevier Ltd. All rights reserved.
http://dx.doi.org/10.1016/j.gca.2013.12.005

1. INTRODUCTION

Cave systems in humid and temperate climates are typically characterised by a distinct seasonality in both external temperature and infiltrating precipitation (affecting ventilation and hydrogeochemical processes), and this seasonality is reflected in the chemical, isotopic and optical compositions of speleothems (Fairchild et al., 2001; Frisia et al., 2011; Fairchild and Baker, 2012;). The role of infiltrating precipitation in influencing speleothem trace element chemistry has been a recent focus of research (Borsato et al., 2007; Fairchild et al., 2010) and is of particular interest because of the identification of trace metal transport by natural organic matter (NOM) in cave dripwaters (Hartland et al., 2011, 2012). In this paper, we investigate the degree to which speleothems capture NOM-metal complexes from solution by focusing on a hyperalkaline system where the aqueous NOM–metal species have been previously characterised (Hartland et al., 2011).

Although rare, hyperalkaline systems in natural caves afford several advantages for the investigation of complexation reactions between NOM and metals, and their subsequent partitioning into speleothems. In particular, there is now a growing body of literature from the dripwaters of Poole's Cavern, Buxton, UK (Hartland et al., 2010b), demonstrating the relevance of the gradation in pH values from pH 8 to 12 within the cave system. Processes observed, include the increased stability of natural organic matter (NOM) in colloidal (1–1000 nm) and particulate (>1000 nm) size ranges arising from electrostatic effects (Hartland et al., 2010a,b); and stronger binding of metals by NOM at increasing pH demonstrated by higher M^{z+}/NOM ratios and slower dissociation kinetics than observed at circum-neutral pH values (Fairchild and Hartland, 2010; Hartland et al., 2011);

This study capitalises on the stronger binding between metals (most notably Co) and NOM in hyperalkaline dripwater PE1 (Hartland et al., 2011) to investigate the partitioning of NOM–metal complexes into the conjugate, fast-growing PC-08-1 stalagmite. High calcite precipitation rates in the speleothem allow very high resolution measurements to be made to resolve seasonal scale variations in NOM and trace elements. In addition, order-of-magnitude higher calcite precipitation rates in this system allow kinetic effects on trace elements to be clearly delineated. We now review the data from experiments and studies of normal (ca. pH 7–8) cave waters and conjugate speleothems before discussing the most relevant information from recent studies at Poole's Cavern.

Indicative data on metal partitioning (expressed as ratio of trace element to Ca ratios in calcite and in solution; Eq. (1)) into speleothems suggest that heavy metals (e.g. Cu, Zn, Y, Pb) behave differently to hydrolysing alkaline earth metals (e.g. Sr, Mg) (Fairchild et al., 2010), but also that partitioning can be substantially different between metal ions with similar binding affinities for humic substances (Benedetti et al., 1996; Milne et al., 2003).

$$K_{\mathrm{d\ app}} = \frac{M^{z+}/Ca^{2+}(s)}{M^{z+}/Ca^{2+}(aq)} \quad (1)$$

where M^{z+} is the trace metal ion, Ca^{2+} is the calcium ion, $K_{\mathrm{d\ app}}$ is the usual, apparent inorganic partition coefficient for the trace metal, which may vary to a lesser or greater extent with temperature, precipitation rate, crystal morphology, or other aspects of solution composition (e.g. complexation reactions between organic ligands and trace ions) (Busenberg and Plummer, 1985; Fairchild and Treble, 2009).

For example, despite empirical distribution coefficients (expressed as ratio of trace element to Ca ratios in calcite and in solution; Eq. (1)) having values of $\gg 1$ predicted by theory (Fairchild and Baker, 2012), in practice, values of $\ll 1$ for Cu and Y, and $\gg 1$ for Zn and Pb have been calculated between dripwaters and stalagmites from Obir cave, Austrian Alps (Fairchild et al., 2010). One possibility is that such differences in partitioning between solution and speleothem reflect variable kinetics of metal dissociation from complexes with NOM, i.e. Cu and Y being more strongly retained in aqueous complexes with NOM than Zn and Pb.

Experimental data on ternary surface complexation reactions (co-adsorption of the ligand and complexed metal at the mineral surface) between NOM–metal complexes and calcite are limited. For example, Lee et al. (2005) studied Cu(II) and fulvic acid adsorption on calcite. They found that adsorption occurs rapidly at mmol Cu(II) concentrations and OC concentrations between 1 and 15 mg L^{-1}, but that dissociation and adsorption of Cu(II) onto calcite occurs preferentially over complex formation with surface-adsorbed fulvic acid (Lee et al., 2005). However, the metal–ligand ratios studied by Lee et al. (2005) were not representative of cave dripwaters or other natural freshwater systems, being much higher with respect to Cu(II) than natural concentrations.

The high affinity of transition metals for calcite surface sites (relative to NOM) may mean that ternary NOM–metal complexes are uncommon in stalagmites. Similarly to Cu(II), both Pb(II) and Zn(II) also display a strong affinity for calcite surfaces, forming inner-sphere complexes (Zachara et al., 1991; Godelitsas et al., 2003; Chada et al., 2005) that are stable over long timeframes (Elzinga et al., 2006). Hence, competitive interactions between metals for binding sites at the calcite surface (following dissociation from NOM ligands) may be an important determinant of the incorporation of colloid-transported metals and other elements in speleothems. One implication of this is that the most weakly-bound fraction of metals held in NOM–metal complexes is likely to be the fraction most readily incorporated in speleothems.

The partitioning of NOM–metal complexes between solution and mineral can be described as a function of the interaction between the aqueous complex and the adsorbed complex at the mineral surface (Fein, 2002). Incorporation of NOM-complexed metals can occur via two mechanisms: ternary complexes (zero partitioning) and non-ternary (partitioning induced by dissociation of NOM–$M_{(aq)}$) complexes. Ternary complexes therefore correspond to co-adsorption and thus for aqueous complexes with high stabilities, the incorporation of NOM–metal complexes in the mineral is expected to occur at a ratio of 1 (Eq. (2)).

$$\equiv SOH^0{}_{(s)} + L - M^{(L^- + m^+)}{}_{(aq)} + H^+{}_{(aq)} \leftrightarrow \equiv S - L - M^{(m-L+1)}{}_{(s)} + H_2O_{(aq)} \quad (2)$$

where ≡S represents a generic, crystallographically bound metal cation, S, at the surface–water interface, and $L - M^{(L^- + M^+)}$ represents the organic acid–cation complex (Fein, 2002). In speleothem-forming systems, where calcite is continually being precipitated from a thin water film at the stalagmite surface, the capture of metal–ligand complexes can be described as part of the overall reaction:

$$L - M^{(L-+m)}{}_{(aq)} + Ca^{2+}{}_{(aq)} + CO_3{}^{2-}{}_{(aq)} \leftrightarrow CaCO_{3(s)+} \equiv L - M^{(L-m^+)}{}_{(s)} \quad (3)$$

Thus, neglecting carbonate, we can define the apparent equilibrium partition coefficient for this reaction as:

$$K_{d\ NOM\text{–}M\ app} = \frac{\equiv L^{l-} - M^{m+}(s)}{Ca^{2+}(s)} \Big/ \frac{L^{l-} - M^{m+}(aq)}{Ca^{2+}(aq)} \quad (4)$$

Within a suite of metals with similarly high binding affinities for calcite surface sites it may be a reasonable approximation to predict that where metal loadings are very low (as in cave waters where concentrations are typically ⩽5 ppb for many metals), differences in the extent of ternary surface complexation between NOM–metal complexes can be attributed to the stability of each aqueous complex, such that:

$$K_{d\ NOM\text{–}M\ act} = \frac{[L^{l-}][M^{m+}](s)}{[Ca^{2+}](s)} \Big/ \frac{[L^{l-}][M^{m+} \cdot f_m](aq)}{[Ca^{2+}](aq)} \quad (5)$$

where f_m the proportion of metal that is free (or is exchangeable over the relevant timescale) defined by:

$$f_m = \frac{[M^{z+}(\text{free})(aq)]}{[M^{z+}(\text{total})(aq)]} \quad (6)$$

Of course, a simple partitioning approach cannot distinguish between the fraction of metal incorporated in ternary complexes and that incorporated as inorganic ions, but does enable the testing of hypotheses about the impact of aqueous complexation reactions on the partitioning of metals and NOM. It should also be acknowledged that additional complexities arise from:

(i) The heterogeneous speciation and size distribution of aqueous NOM and metals (Lead and Wilkinson, 2006; Aiken et al., 2011).
(ii) The variability in NOM-metal transport in caves that arises from the interaction between infiltration, flow routing, and the hydrodynamic properties of the fine colloids and particulates (Hartland et al., 2012).
(iii) Variable dissociation kinetics through time as a function of (a) (Hartland et al., 2011).
(iv) The surface charge of calcite and the availability of $CaCO_3$ lattice sites as well as increased incidence of crystallographic defects with implications for incorporation of a range of trace species (Fairchild and Treble, 2009; Fairchild and Hartland, 2010).

Thus, incorporation in speleothem calcite with consistent surface site properties will be determined by:

(i) The size and composition (i.e. hydrophilicity/hydrophobicity) of the NOM ligand, affecting adsorption and stability at the calcite surface.
(ii) The lability (i.e. exchangeability) of the complexed metal and its binding affinity for the calcite surface.
(iii) The concentration of aqueous complexes.

Given the complexities, a partitioning approach to the problem is appropriate as a first approximation rather than a precise description. This study seeks to make the first quantitative connection between the organic and inorganic compositions of speleothems and thus determine the potential for speleothems to encode fluctuations in colloid-facilitated trace metal transport in karst aquifers.

1.1. Recent findings of direct relevance to the present study

The conjugate dripwater (PE1) to the stalagmite studied here (PC-08-1) was characterised in June 2009 using an array of complementary techniques, in which the size, speciation and lability of NOM–metal complexes was characterised (Hartland et al., 2011), where lability is defined as the capacity for complexes to dissociate in the context of the on-going interfacial process at the stalagmite surface. In PE1 dripwater, the most stable aqueous complexes were formed between Co and the finest, low molecular weight component of the NOM spectrum (Hartland et al., 2011). Speciation experiments demonstrated that Co was essentially non-exchangeable (free metal (f_m) = <0.05), being retained in aqueous complexes, whilst Cu, Ni and V were all predominantly bound by NOM (f_m = 0.2–0.3).In contrast, Sr and Ba were freely exchangeable between the solution and solid phase (Hartland et al., 2011) and Mg was absent, presumably due to the poor solubility of $Mg(OH)_2$ at hyperalkaline pH ($K_{sp} = 1.5 \times 10^{-11}$):

$$Mg^{2+}{}_{(aq)} + 2OH^-{}_{(aq)} \leftrightarrow Mg(OH)_{2(s)} \quad (7)$$

On the other hand, the transition metals were not lost as insoluble hydroxides (Hartland et al., 2012), despite having lower solubility than Mg (e.g. $Cu(OH)_2$ $K_{sp} = 2.2 \times 10^{-20}$); and this is consistent with the dominant role of NOM in solubilising and transporting the transition metals in this system (Hartland et al., 2011).

The transport of metals by complexes with NOM in PE1 dripwater through the hydrological year was studied by Hartland et al. (2012). This study had two findings of direct relevance to the study of trace metal variations in the conjugate PC-08-1 stalagmite:

(i) Complexes between metals and the smallest, low-molecular weight fraction of NOM showed an attenuated delivery in dripwaters consistent with the non-conservative behaviour of analogous tracers in fractured-rock studies due to diffusion into microfractures. This mode of transport was termed 'low-flux' and was the dominant mode of transport for Co and V.
(ii) Complexes between metals and coarse colloids (>100 nm) and particulates (>1000 nm) showed a rapid responsiveness to infiltration events. This was

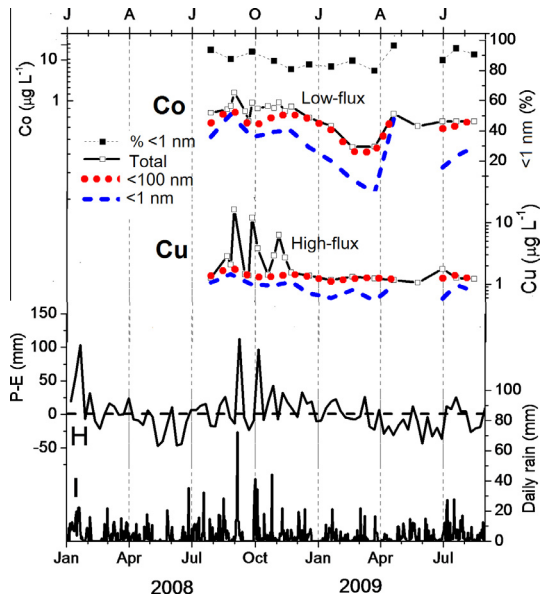

Fig. 1. Summary of low-flux and high-flux behaviour of NOM–metal complexes in PE1 dripwaters, Poole's Cavern (modified from Hartland et al., 2012). The low-flux mode of transport (Hartland et al., 2012) corresponded to the slower migration of fine-colloidal (<100 nm) to nominally-dissolved (<1 nm) NOM. Attenuated delivery of Co and V was attributed to enhanced diffusion into micro-fractures compared to larger colloids (>100 nm) and particulates (>1 µm) corresponding to the high-flux mode transport for Cu, Zn and Ni. Both modes represent extremes in a continuum of hydrodynamic sizes of NOM and although Cu, Zn and Ni preferentially partitioned into the coarse colloidal and particulate size range, they were also complexed to a lesser degree by fine colloidal and nominally dissolved NOM (Hartland et al., 2012).

termed the 'high-flux' mode of NOM-metal transport and was interpreted as being dominantly fracture-fed. This mode of transport was dominated by Cu, Zn and Ni.

The 'high-flux' vs 'low-flux' interplay of trace metal transport is summarised in Fig. 1.

The PC-08-1 stalagmite studied here was deposited following the removal of stalagmite PC-97-1 studied by Baker et al. (1999b) and which grew under the PE1 drip point between 1927 and 1997. Both the PC-97-1 stalagmite and its regrowth (PC-08-1) are characterised by annual lamina couplets consisting of a porous pale layer and a dense fluorescent layer. Fluorescence in the PC-97-1 stalagmite displayed a marked sinusoidal pattern with 10% of laminae exhibiting a double band structure (Baker et al., 1999b).

2. MATERIALS AND METHODS

2.1. Study site

The data for this study were obtained from samples collected from Poole's Cavern (53°12′N 1°56′W), Buxton, UK. The cave was described in detail in Hartland et al. (2010b) and the geochemical composition of monitored dripwaters and their hydrology is examined in Hartland et al. (2012). In this study, trace metal and total organic carbon concentration (TOC) data from the PE1 drip point are compared to trace element and TOC data from the PC-08-1 conjugate stalagmite (Fig. 1). This stalagmite grew on the stump of 20th century sample PC-97-1 whose fluorescence characteristics were described by Baker et al. (1999b).

2.1.1. Impact of hyperalkaline conditions on speleothem deposition

Above pH 9.5, the conventional mechanism of carbonate precipitation is overturned and $CaCO_3$ precipitates via the overall reaction:

$$Ca^{2+}{}_{(aq)} + CO_{2(g)} + OH^{-}{}_{(aq)} \rightarrow CaCO_{3(s)} + H^{+}{}_{(aq)} \quad (8)$$

Because the dissolved carbonate load in hyperalkaline dripwater is typically too low to allow equilibration with respect to the pCO_2 of cave air, $CO_{2(g)}$ is sequestered and combines with OH^- via hydroxylation to $HCO^-{}_3$, which following the loss of H^+, then combines with Ca^{2+} to form $CaCO_3$.During the essentially irreversible hydroxylation reaction ($CO_2 + OH^- \rightarrow HCO^-{}_3$) there is strong depletion in ^{13}C (Clark et al., 1992); this coupled with the strong isotope depletion of ^{18}O associated with the reactant OH^- (40‰ lighter than water) results in very light oxygen and carbon isotope ratios in hyperalkaline carbonates (Clark et al., 1992). Both $\delta^{13}C$ and $\delta^{18}O$ have been found to be much lighter in the pale PC-08-1 lamine than in dark laminae (Hartland et al., 2010b). This can be explained by a combination of light CO_2 sources in cave air and strong kinetic fractionation resulting from higher calcite precipitation rates at high cave air pCO_2 (Hartland et al., 2010b). High cave air pCO_2 values were observed in the summer and autumn (peaking in August) indicating that the pale calcite with low delta values corresponds to faster calcite precipitation in summer resulting from faster CO_2 ingress into solution (and faster reaction kinetics).

2.2. PC-08-1 stalagmite

The PC-08-1 stalagmite (Fig. 2) is a hyperalkaline speleothem which grew between 1997 and June 2008. The stalagmite was sampled in June 2008 and sectioned using distilled water without additional lubricants. The sectioned sample was then polished and cleaned by sequential ultra-sonication in methanol and deionised water to remove contaminants. In PC-08-1, nine pale/dark lamina couplets were discernible comprising the period 1999–2008 (Fig. 2a). Some disruption of deposition may have occurred during early growth (1997–1999) because of regular sampling by previous workers (Baker et al., 1999b). At the time of collection (June 2008) the newly-deposited fabric was pale, porous calcite, overlying a darker, dense band, thus confirming that pale laminae in the sample correspond to summer growth and darker laminae correspond to winter growth (Baker et al., 1999b). Although the pale and dark layers are evident at low magnifications, the boundary between them is not a sharp feature, and there is considerable lateral variation in lamina colour (Fig. 2a). From measurement of the thickness of successive lamina couplets the

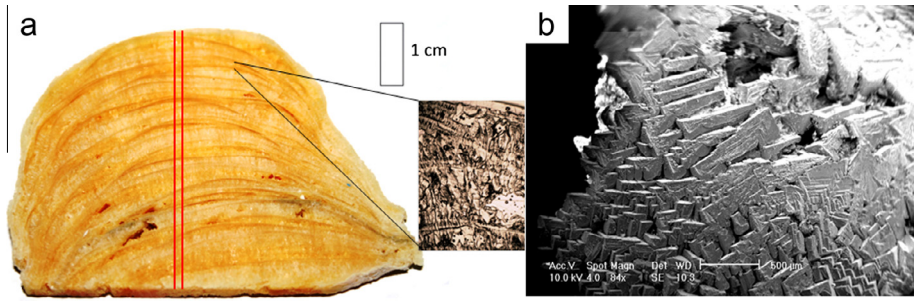

Fig. 2. Sectioned and polished PC-08-1 stalagmite showing successive pale and dark layers (a). Some convex laminae which intersect seasonal layers under polarized light are shown in the enlargement. Red lines mark the location of parallel LA-ICPMS tracks. (b) Scanning electron micrograph of the growth surface of PE1 showing complex aggregates of rhombohedra with growth focused on crystal edges, reflective of rapid, diffusion-controlled precipitation. At around 10–11 mm from the base of the sample there is a highly porous, detritus-rich zone which corresponds to a period of substantial surface disturbance above the cave during which dripwater fluorescence was monitored continuously (Hartland et al., 2010b). (For interpretation of the references to colour in this figure legend, the reader is referred to the web version of this article.)

average vertical extension rate is estimated at ca. 4 mm yr^{-1}, comparable to that of the PC-97–1 stalagmite (ca. 5 mm yr^{-1}), which grew under the PE1 drip point between 1927 and 1997 (Baker et al., 1999b). Average pH and EC values measured in PE1 dripwater between June 2008 and August 2009 were 11.7 ± 0.4 and 0.7 ± 0.24 mS cm^{-1}, respectively. Intra-annual variations in calcite precipitation rate, driven by changes in drip rate and cave air pCO_2, have the potential to influence the partitioning behaviour of NOM–metal complexes and this is considered here.

The fluorescent properties of the PC-97-1 stalagmite and its parent waters were studied by Baker et al. (1999b), who identified the occurrence of autumn/winter fluorescence maxima with respect to the humic-like peak C fluorophore. Both the PC-97-1 stalagmite and its regrowth (PC-08-1) are characterised by annual lamina couplets consisting of a porous pale layer and a dense fluorescent layer. Fluorescence in the PC-97-1 stalagmite displayed a marked sinusoidal pattern with 10% of laminae exhibiting a double band structure (Baker et al., 1999b).

Annual lamina couplets in the PC-08-1 sample (formed approximately parallel to the stalagmite growth surface) are intersected by arcs of columnar calcite (highlighted in Fig. 2) which are often more convex than the pale-fluorescent lamina couplets (Fig. 2). These arcs grow sideways rather than representing simultaneous growth laminae (Hartland et al., 2010b). The migrating position of the centre of each convex layer may be driven by rapid changes in the position of the feeding soda straw, which also show very high precipitation rates.

2.2.1. PC-08-1 primary mineralogy and precipitation mechanism

SEM images of the top surface of the PE1 sample demonstrate that the precipitation style is as complex aggregates of rhombohedra. Typically, there is preferential development of crystal edges (Fig. 2b) which represents an incipient skeletal morphology (Sunagawa, 2005). This is consistent with an origin from growth limited by diffusion of carbon dioxide in the solution film towards crystals (Supporting information). Crucially, there is no morphological hint of any amorphous $CaCO_3$ or metastable (e.g. vaterite) precursor phases. Hence it would be expected that the crystals should be interpreted as primary calcites displaying kinetic controls on their chemical composition.

2.3. PC-08-1 chronology

Counting back from June 2008, nine pale/dark lamina couplets are visible corresponding to the period summer/winter 1999/2000 to 2007/2008. Uncertainties relating to intra-annual calcite precipitation rate variations over this period mean that it is difficult to derive a precise chronology. Certain assumptions and simplifications must therefore be made. Because stable isotopes were most strongly kinetically fractionated in pale laminae (Section 3.1), the assumption was made that higher calcite precipitation rates during deposition of pale laminae corresponded to higher cave air pCO_2 values between May and October of each year. This is based on measurements of cave air pCO_2 in the Poached Egg chamber of Poole's Cavern between October 2008 and August 2009 (Hartland et al., 2010b), but also on observing the stalagmite in relation to its month of collection. Variations in PC-08-1 precipitation rate within pale/dark laminae are not accounted for because of uncertainties in the relation between cave air pCO_2, drip hydrology and calcite precipitation rate. However, the difference between the precipitation rate of dark and pale laminae is considered to more important because intra-lamina $\delta^{13}C$ and $\delta^{18}O$ variability (reflecting kinetic fractionation) is of a much lower-order than inter-lamina variability (Fig. 3). This simplification does not allow for variations in drip rate above the baseline of 2–3 drips per minute, mainly because the recorded excursions from the baseline discharge were non-linear and did not coherently relate to variations in infiltration or solution chemistry (Hartland et al., 2012). High discharge events at drip PE1 were typically short-lived (<24 h duration), however one longer period of high discharge was recorded. Discharge during this period varied between 0.1 and 150 drips per minute for ca. 1 month duration, as recorded by drip loggers. This was the only sustained period of elevated discharge in over 13 months of continuous drip rate data (Hartland et al., 2012).

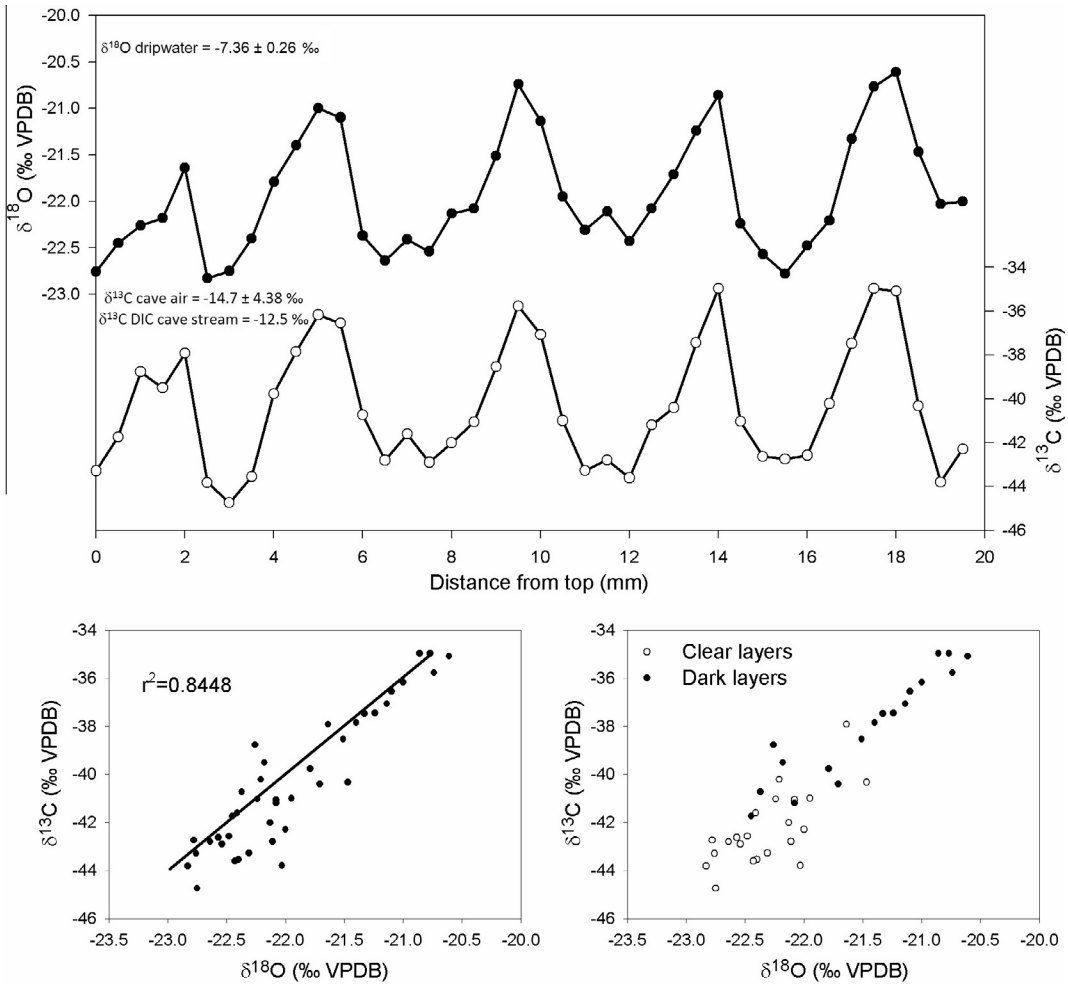

Fig. 3. Stable isotope record of the top 20 mm of the PC-08-1 stalagmite, isotope ratios correlation and isotope signature of clear and dark layers. When the stalagmite was collected (summer 2008) pale calcite was being deposited. High cave air pCO_2 values are observed in the summer and autumn (peaking in August) coinciding with deposition of pale calcite and low delta values (measured in monthly-collected precipitates). This corresponds to faster calcite precipitation in summer resulting from faster CO_2 ingress into solution (and faster reaction kinetics).

Because the boundary between pale and dark layers is not a sharp feature and because there is considerable lateral variation in lamina colour, visual delineation of pale and dark laminae was not considered to be the most reliable approach. Instead, trace element variations were used to delineate winter growth from summer growth (both Co and V are enriched in dripwaters in the winter). This was possible because the trace metals V and Co showed distinct antipathetic variance with Sr and Ba. Of these elements, V and Sr showed the clearest association with growth fabric: V being enriched in dark laminae and Sr being enriched in pale laminae (Supplementary Fig. 3). Thus, the boundary between pale and dark laminae was designated as the median V/Sr value in adjacent laminae.

2.4. Chemical analysis of PE1 dripwater and PC-08-1 stalagmite

2.4.1. Organic matter in dripwater and calcite

TOC concentrations were determined using a Shimadzu (Kyoto, Japan) TOC-V high-temperature combustion analyser following the non-purgable organic carbon (NPOC) method. All glassware was cleaned by soaking in 10% HNO_3 and deionised water (DIW) and organic carbon (OC) was removed by combustion at 500 °C for 5 h. Concentrations in size-fractionated dripwater samples were determined by taking the average of between 3 and 8 injections (2 washes, 3 min sparge). Stalagmite powders were obtained using a diamond-tipped hand drill. Samples from alternating pale and dark layers (~100 mg) were dissolved in 1 mL 2 M Ultrapure HCl and diluted 10 times with deionised water prior to analysis using between 3 and 5 injections. Carbonate samples were sparged with O_2 for 5 min to remove any residual inorganic carbon. Carbonate TOC procedural blanks were also prepared using Aristar $CaCO_3$ and had average TOC contents of 0.02 ± 0.02 mg g^{-1}. Reported values for TOC in the PC-08-1 stalagmite are blank-corrected using this value. In addition to TOC analyses, dissolution samples of PC-08-1 were analysed using fluorescence EEMs constructed by the standard methods outlined in (Hartland et al., 2010a).

2.4.2. Trace element composition of the PC-08-1 stalagmite

ICP-MS analysis of dripwaters and PC-08-1 dissolutions was performed on an Agilent quadrupole ICP-MS. Powdered stalagmite samples (ca. 2 mg) were dissolved in 1.6 mL 10% Aristar HNO_3 and then diluted with 6.4 mL DIW (producing a sample matrix of 2% HNO_3 and 100 mg L^{-1} Ca). Calibration standards were matrix matched to 100 mg L^{-1} Ca and 10, 20 and 50 mg L^{-1} check standards were analysed at regular intervals during each run. Isotopes measured were ^{23}Na, ^{24}Mg, ^{27}Al, ^{29}Si, ^{47}Ti, ^{51}V, ^{52}Cr, ^{55}Mn, ^{56}Fe, ^{59}Co, ^{60}Ni, ^{63}Cu, ^{66}Zn, ^{79}Br, ^{88}Sr, ^{89}Y, ^{114}Cd, ^{137}Ba, and ^{208}Pb. Concentrations of Cd and Y in stalagmite dissolutions were below detection limits (<0.2 μg L^{-1}).

Spatially-resolved (trace) element concentrations in the PC-08-1 stalagmite were measured along two parallel tracks (300 μm spacing) along the growth axis via laser ablation ICPMS (LA-ICPMS). Analysis was performed at Royal Holloway University of London using a custom-built excimer 193 nm laser-ablation system (RESOlution M-50 prototype, Resonetics LLC, USA) featuring a two-volume laser-ablation cell (Laurin Technic, Australia) coupled to an Agilent 7500ce quadrupole ICPMS (described in detail in Muller et al., 2009). The sample was initially pre-ablated with two passes (96 μm spot, 50 Hz, 30 mm/min) as a cleaning step, whereas data acquisition utilized 74 μm, 15 Hz and 2 mm/min in continuous profiling rather than discrete spot mode at a laser fluence on target of ~4 J/cm^2. Ablation took place in a He atmosphere (850 ml/min continuous He flow) to which both Ar (~450 ml/min) and N_2 (6 ml/min) were added downstream of the LA cell; the signal smoothing device ('squid') was included. Tuning of the ICPMS ensured maximum signal to background ratio while maintaining ThO/Th < 0.3% and ^{232}Th/^{238}U > 90%. The following masses (m/z) were measured: ^{23}Na, ^{25}Mg, ^{27}Al, ^{31}P, ^{43}Ca, ^{47}Ti, ^{51}V, ^{53}Cr, ^{55}Mn, ^{57}Fe, ^{59}Co, ^{60}Ni, ^{65}Cu, ^{66}Zn, ^{79}Br, ^{88}Sr, ^{89}Y, ^{138}Ba, ^{139}La, ^{140}Ce, ^{208}Pb and ^{238}U with dwell times ranging between 10 and 50 ms and an overall sweep time of ~730 ms; we focus here predominately on results from elements V, Co, Ni, Cu, Zn, Br, Sr, Ba and Pb. NIST612 was used as external standard for quantification (following (Longerich et al., 1996)) and pressed powder carbonate standard pellet USGS MACS3 as secondary carbonate to assess accuracy, which typically ranges between 1% and 8% for the elements reported herein. Ca was used as internal standard and all reported concentrations are based on a stoichiometric Ca concentration in $CaCO_3$ of 40% m/m. This method produces ~42 analyses per mm, enabling trace element concentrations in the samples to be determined at a spatial resolution of ca. 70 measurements per year.

2.5. Stable isotope analysis of PC-08-1

The oxygen and carbon stable isotopes (δ^{18}O and δ^{13}C) of the speleothem calcite were analyzed along a section covering 20 mm from the top of the sample in order to characterize the isotopic pattern of several laminae (i.e. pale and dark layers). The considered section was along the vertical axis of the stalagmite in a central position. The sampling was carried out with a hand micro-drill equipped with a tungsten burr of 0.5 mm tip diameter. Before each sample collection the drill bit was rinsed in 10% HCl and methanol and the stalagmite was blown with compressed air to prevent powder contamination from previous samples. The sampling was conducted with a 0.5 mm spatial resolution in a parallel double row in order to avoid cross-contamination. This sampling protocol provides a continuous record although potential for some overlapping of contiguous samples is not discounted.

An average sample size of 103 ± 10 μg was analyzed in an Isoprime-IRMS equipped with a multiflow autosampler at the University of Birmingham. The internal analytical uncertainties were 0.13‰ for δ^{18}O and 0.04‰ for δ^{13}C. The isotope data were calculated using a double point calibration method using NBS-18 and NBS-19 IAEA standards after correcting the run drift with internal reference samples of Carrara marble.

3. RESULTS AND DISCUSSION

3.1. Isotopic composition of PC-08-1 stalagmite

Petrographic seasonality between pale porous calcite and dark dense calcite is shown clearly in Fig. 2. This seasonality is matched by variations in both carbon and oxygen isotopes which are well correlated (Fig. 3). Isotopic compositions are heavier in dark layers and lighter in pale porous layers, confirming kinetic fractionation at high precipitation rates when the pCO_2 of cave air is seasonally high (summer). This clear kinetic fractionation between pale and dark calcite is used here to investigate the effects of calcite precipitation rate on the incorporation of trace species.

3.2. Incorporation of NOM into the speleothem

Organic carbon (OC) concentrations in PC-08-1 were somewhat higher than in the range of other cave samples analysed (Table 1), varying between 0.2 and 1.6 mg g^{-1} of calcite (Fig. 4c). Indeed, OC concentrations in PC-08-1 were two times higher than the next most organic-rich sample (Table 1). This is consistent with the generally higher OC concentrations in hyperalkaline dripwaters at this site, previously attributed to electrostatic stabilisation of NOM at high pH (Hartland et al., 2010a,b).

Stalagmite fluorescence has been examined by the non-perturbing methods of fluorescence microscopy (Baker et al., 1993) and scanning fluorescence spectroscopy (Baker et al., 1999a), but aqueous stalagmite dissolutions have not been previously characterised using fluorescence Emission Excitation Matrices (EEMs). The results of the fluorescence analyses demonstrate that the fluorescent characteristics of NOM released from stalagmite laminae closely resemble the dripwater NOM signal (Hartland et al., 2010a) with no apparent compositional differences evident between laminae (Fig. 4a andb).

Fluorescence analysis of dissolutions of laminae cannot be quantitatively compared to analyses in dripwaters because of several factors, including their high Ca^{2+} and OC concentrations. However, the TOC and fluorescence

Table 1
Average organic and elemental compositions of selected stalagmites. Trace elements determined by solution ICPMS analysis of stalagmite dissolutions prepared following the procedure described in Section 2.4.

		Values in ppm/calcite																	
Sample	Site	TOC (%)	±	Mg	±	Al	±	Ti	±	V	±	Cr	±	Mn	±	Fe	±	Co	±
OBI-84	Obir, Austrian Alps	0.01	0.00	1096	15	38	15	–	–	–	–	–	–	1.0	*	116	186	–	–
ER-77	Ernesto, Italian Alps	0.05	0.01	732	62	32	62	–	–	–	–	–	–	–	–	21	4.7	0.1	0.1
PC-08-1	Poole's Cavern, UK	0.09	0.06	–	–	113	60	0.3	0.5	27.2	6.1	0.5	0.3	2.0	0.7	22	8.8	0.2	0.0
→Pale		0.11	0.08	–	–	101	52	0.4	0.6	24.6	6.3	0.5	0.4	2.7	–	21	9.4	0.2	0.1
→Dark		0.07	0.02	–	–	128	68	0.2	0.2	30.4	4.2	0.5	0.2	1.6	0.4	23	8.5	0.2	0.0
LBM-1	Lower Balls Green Mine, UK	0.05	0.01	41	17	–	–	–	–	–	–	1.5	0.3			44	12	0.0	0.0
		Ni	±	Cu	±	Zn	±	Br	±	Sr	±	Y	±	Cd	±	Ba	±	Pb	
OBI-84	Obir, Austrian Alps	3.7	0.6	10	2.9	4806*	1192	6.6	3.0	24	1.1	–	–	2.9	0.2	168	6	748	48
ER-77	Ernesto, Italian Alps	20	24	11	3.2	17	9	4.5	0.4	10	0.4	1.5	0.1	0.7	0.6	4.2	3.7	1.8	0.5
PC-08-1	Poole's Cavern, UK	5.7	4.5	15	16	12	13	3.0	1.2	120	11	–	–	–	–	50	3	4	2
→Pale		4.3	0.8	18	22	11	15	2.5	1.2	124	13	–	–	–	–	51	3.9	3.5	1.2
→Dark		7.3	6.5	12	4.0	13	10	3.7	0.8	114	5.3	–	–	–	–	49	2.5	4.2	2.0
LBM-1	Lower Balls Green Mine, UK	25	26	13	6.5	11	8.1	4.6	0.5	74	1.8	–	–	–	–	5.0	0.4	1.0	0.2

'–' denotes an analysis below the limits of detection.
* Zn value is from Obir stalagmites OBI-84 from Fairchild et al. (2010).

data (Fig. 4c and d) indicate that fluorescence was marginally higher in dark laminae, consistent with stalagmite PC-97-1 (Baker et al., 1999b), and OC generally more concentrated in pale laminae. With respect to several trace elements (e.g. Cu, Ni, Al, Fe, Cr, Pb), the compositions of dark and pale laminae dissolutions were found to be similar. Although darker layers contained marginally higher concentrations of Cu, Ni, Al and Pb, there was no clear systematic association with fabric type (Table 1). Contrastingly, darker laminae were characterised by clear enrichments in Co, V and Br, and marked depletion in Sr, and to a lesser extent, Ba.

3.3. Potential effects of hyperalkaline deposition on NOM–metal partitioning

The solution chemistry of hyperalkaline dripwater PE1 changes rapidly as a result of the reaction between $CO_{2(g)}$, $OH^-_{(aq)}$ and $Ca^{2+}_{(aq)}$ which proceeds effectively instantaneously and results in a dramatic drop in pH and Ca^{2+} concentration (Fig. 5) because of the high surface area to volume (SA/V) ratio of the thin film at the stalagmite surface. Modelling of calcite deposition (Fig. 5 and Supporting information) in PC-08-1 demonstrates that around 20% of Ca is removed from solution in ca. 15 s, which is reasonably consistent with the calculated efficiency of Ca removal of 20% in PC-08-1 (Hartland et al., 2010b) and the average interval between drips at drip point PE1 is 20–25 s (Baker et al., 1999b; Hartland et al., 2012), given the uncertainties involved.

Modelling of Cu^{2+} binding with dissolved organic matter (DOM) using the speciation code Visual MINTEQ 3.0 demonstrates that although solution pH changes rapidly during calcite deposition from hyperalkaline dripwater, strong binding of Cu^{2+} by DOM should theoretically be slightly enhanced because of a reduction in competition from Ca^{2+} (Fig. 5b). Thus, changes in solution chemistry during deposition are unlikely to have influenced the partitioning of the transition metals from aqueous complexes with NOM.

3.4. Partitioning of NOM–metal complexes between solution and speleothem

The partitioning of OC and trace metals between PE1 dripwater and PC-08-1 stalagmite was examined for a group of metals (Cu, Ni, V, and Co) which have been shown to form aqueous complexes with NOM in hyperalkaline dripwater and which exhibit a range of stabilities (i.e. their tendency to remain as complexes and not dissociate) (Hartland et al., 2011). Partitioning of trace elements and NOM into the speleothem was assessed using the trace metal (Tr) and organic carbon (OC) concentrations in the stalagmite and concentrations in dripwater (Hartland et al., 2011, 2012).

If we temporarily disregard the organic component in Eq. (8), this can be simplified to give the usual inorganic partition coefficient for the trace metal (Eq. (1)) and the partition coefficient with an additional factor allowing for the fraction of free metal in solution:

$$K_{\mathrm{d\ act}} = \frac{M^{2+}/Ca^{2+}(s)}{[M^{2+} \cdot f_m]/Ca^{2+}(aq)} \tag{9}$$

where M^{z+} is the trace metal ion, f_m is the free metal fraction, K_d is the distribution coefficient, which may vary to a lesser or greater extent with temperature, precipitation rate, crystal morphology, or other aspects of solution composition (e.g. complexation reactions between organic ligands and trace ions) (Busenberg and Plummer, 1985; Fairchild and Treble, 2009).

Results for the inorganic apparent $K_{d\ app}$ (Eq. (1)) values for the metals Co, V, Ni and Cu are 0.05, 0.22, 0.36 and 0.62. Hence, the hierarchy of K_d values is Co $\ll$ V $<$ Ni $<$ Cu, is broadly in accord with the hierarchy of free metal

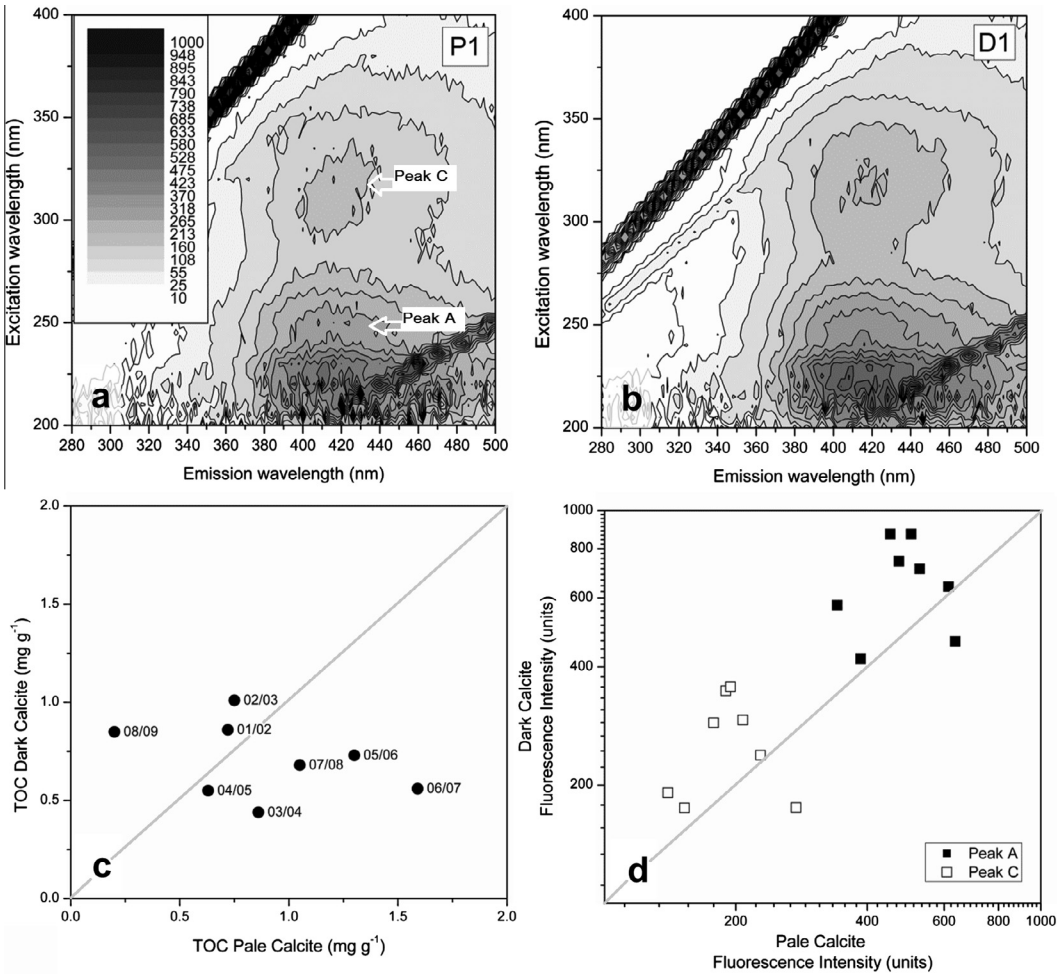

Fig. 4. Fluorescence three dimensional emission excitation spectra (EEM) and total organic carbon (TOC) data from calcite dissolutions of PC-08-1 lamina (a) pale (P) layer #1 (b) dark (D) layer #1 (c) TOC in mg g^{-1} in pale and dark calcite (d) fluorescence intensities in pale and dark layers for the peak C and peak A fluorophores. For designations of peak fluorescence centres see Hartland et al. (2011).

concentrations (given here as fractions) measured in the dripwater for the aqueous NOM–M complexes (Hartland et al., 2011), as follows $0.04 \ll 0.23$, 0.28 and 0.23, respectively. If we then calculate the inorganic partition coefficients, factoring in the available, or 'free', metal concentrations (f_m) to give $K_{d\ act}$ (Eq. (9)) we obtain values for Co, V, Ni and Cu as follows: 1.65, 1.15, 2.63 and 2.90. Hence, the $K_{d\ act}$ values for Ni and Cu are very similar, which is in accordance with the generally high affinities of transition metal ions for inner-sphere surface complexation with calcite under purely inorganic conditions (Zachara et al., 1991; Godelitsas et al., 2003; Chada et al., 2005). Of course, the $K_{d\ act}$ values do not apply in a mechanistic sense, since we cannot assume that all of the trace metal was substituted for Ca^{2+} at lattice sites, and no ternary complexation occurred. A sensitivity analysis (Fig. 6) shows the importance of free metal concentration on values of $K_{d\ app}$.(free metal concentrations taken from Hartland et al., 2011). At 100% free metal (the usual implicit assumption for $K_{d\ app}$ values) the K_d values are widely divergent (Fig. 6). However, allowing for the measured f_m value it is clear that the calculated $K_{d\ act}$ values (circular symbols, Fig. 6) for Co and V (low-flux) and Cu and Ni (high-flux) are much more closely clustered.

Now considering the organic component in this system, the partition coefficient ($K_{d\ NOM}$) for the surface complexation reaction between aqueous NOM and the calcite surface described in Eq. (1) may be reformulated as:

$$K_{d\ NOM} = \frac{NOM/Ca^{2+}(s)}{NOM/Ca^{2+}(aq)} \tag{10}$$

Substituting in TOC values in dripwater and calcite a $K_{d\ NOM}$ value of 0.033 is obtained for PC-08-1, equating to a putative NOM removal efficiency of 3.3%. Thus, NOM is incorporated in the stalagmite much less readily than the transition metals with the exception of Co which has a comparable $K_{d\ app}$ value of 0.061. The partitioning of NOM–M complexes can then be estimated as follows:

$$K_{d\ NOM\text{–}M\ app} = \frac{M^{2+}/NOM(s)}{M^{2+}/NOM(aq)} \tag{11}$$

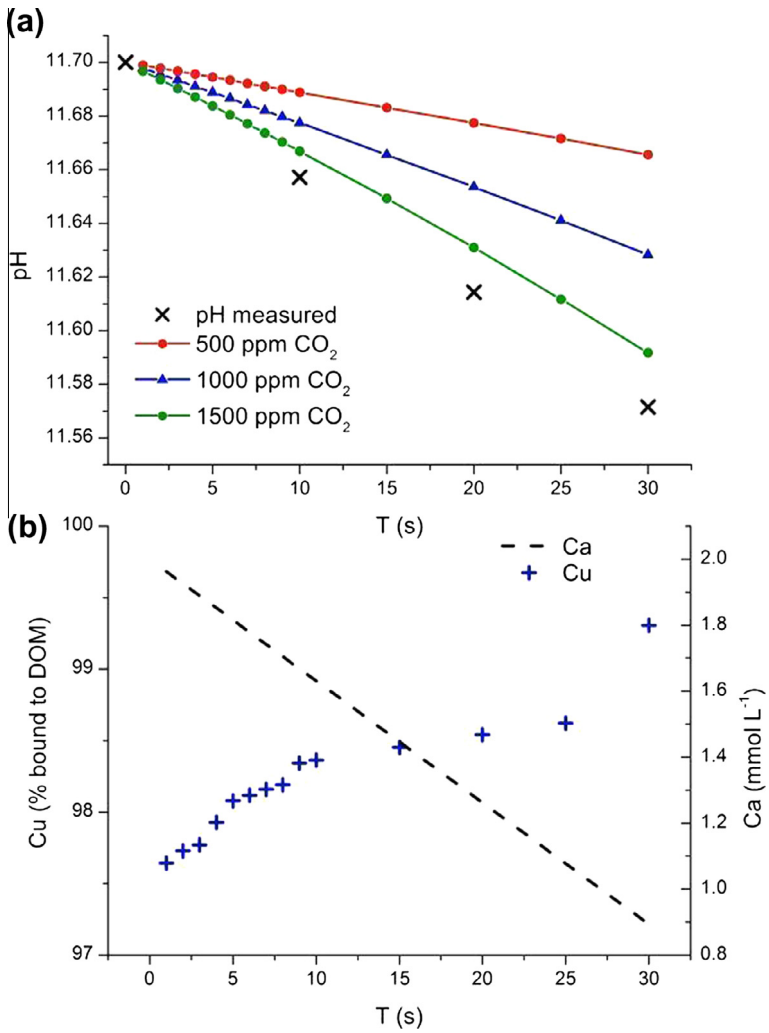

Fig. 5. Modelled change in PE1 dripwater composition during the precipitation of calcite as driven by $CO_{2(g)}$ ingress into solution under hyperalkaline conditions (a) pH change under varying cave air pCO_2 values; (b) change in Ca(II) and the fraction of Cu(II) complexed by humic acid simulated using the MINTEQ modelling code. For details of the modelling approach taken see the Supporting information.

The $K_{d\ NOM\text{–}M\ app}$ values are obtained for Co, V, Ni and Cu are given in Table 2. This is consistent with the previous findings and shows that more labile NOM–M complexes have higher values of $K_{d\ NOM\text{–}M\ app}$. Thus, the ratio of metal-to-ligand (taking TOC as a crude measure of the total ligand concentration) in the stalagmite is much higher than in the water, with the exception of NOM-Co which has a mean $K_{d\ NOM\text{–}M\ app}$ of 0.9. It is clear that NOM–Co partitions at lower ratios in the dark (winter) calcite compared to the pale (summer) calcite. Since petrographic seasonality is related to calcite precipitation rate, which is higher at elevated pCO_2 (summer in Poole's Cavern, Hartland et al., 2010b) in hyperalkaline carbonates (Clark et al., 1992), this indicates a precipitation rate effect on partitioning, i.e. at lower precipitation rates the time available for dissociation of NOM–M complexes is increased and thus, $K_{d\ NOM\text{–}M\ app}$ ratios increase accordingly.

In general, the partitioning process therefore favours incorporation of metals over organic ligands, and the most labile metals with high affinities for binding with calcite therefore become preferentially incorporated. This may correspond to a situation commonly found in stalagmites, where discrete trace metal enrichments associated with organic complexation are identified, but luminescence (auto-fluorescence) of the associated calcite is weak (Fairchild et al., 2010). This analysis implies that where a metal such as Co is strongly complexed in aqueous solution, incorporation in the stalagmite is primarily through ternary surface complexation (Fig. 7), but that this is the exception rather than the rule.

Ternary complexation therefore places a limit on the incorporation of strongly bound metals since this process is limited by the slower diffusion of NOM–M relative to inorganic species, and by other complicated reaction mechanisms (e.g. calcite surface charge modification, electrostatic interactions between ligands, hydrophobic interactions between ligands, steric effects, etc. (Murphy et al., 1990)). In Fig. 7, the range of Co to organic carbon concentrations in dripwater (passing a ca. 100 nm filter membrane) and stalagmite are shown. Cobalt in Poole's

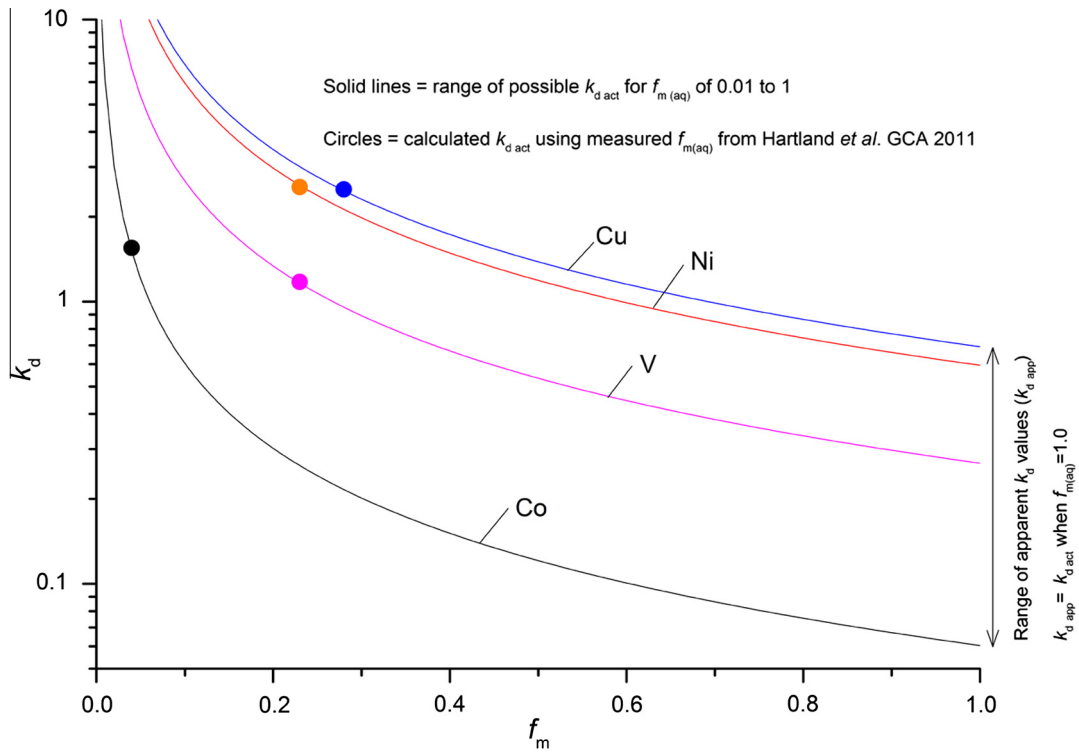

Fig. 6. The effect of the free (or exchangeable) metal ion fraction (f_m) on the K_d value of the actual trace metal inorganic partition coefficient ($K_{d\ act}$) between PE1 dripwaters and the PC-08-1 stalagmite. When free metal ion concentrations measured by Hartland et al. (2011) (shown by the position of circular symbols) are taken into account, the actual K_d values of the transition metals cluster suggesting similar affinities for incorporation in calcite. In particular, note the similar behaviour of Cu and Ni and Co and V, respectively. The usual, apparent partition coefficient ($K_{d\ app}$) value for this system corresponds to $f_m = 1.0$ at which point and $K_{d\ app}$ and $K_{d\ act}$ have the same value. This sensitivity analysis shows that much of the variance in apparent transition metal partitioning behaviour in natural systems can be accounted for by complexation reactions between natural organic ligands and these metals in dripwaters.

Table 2
Calculated partition coefficients for NOM-M complexes in hyperalkaline stalagmite PC-08-1.

	K_d	Element					K_d
		Co	V	Ni	Cu		
Average	Inorg-app	0.06	0.27	0.68	0.74		NOM
	Inorg-act	1.68	1.15	2.90	2.63	Average	0.03
Pale	Inorg-app	0.05	0.23	0.36	0.62	Pale	0.04
	Inorg-act	1.45	0.98	1.54	2.20	Dark	0.03
Dark	Inorg-app	0.07	0.31	1.00	0.86		
	Inorg-act	1.91	1.32	4.26	3.05		
Average	NOM–M app	0.9	32	105	146		
Pale		0.7	24	67	145		
Dark		1.4	47	177	148		

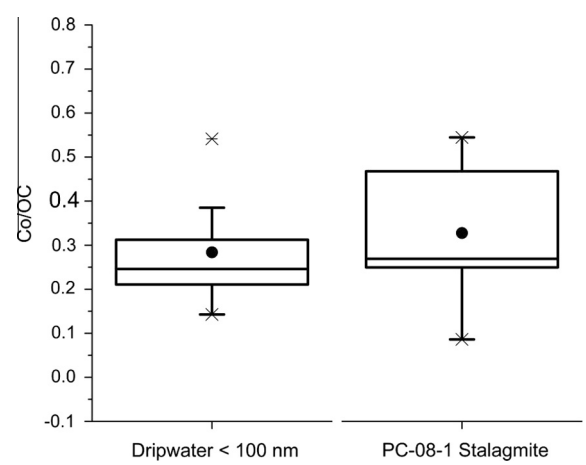

Fig. 7. Box plot showing the ratios of cobalt (Co) to organic carbon (OC) in 100 kDa (ca. 100 nm) filtered dripwater samples and in the conjugate stalagmite PC-08-1. Ratios occupied a similar range in dripwater and speleothem, the median and mean values being slightly higher in the stalagmite consistent with minor dissociation of Co complexes during incorporation.

Cavern hyperalkaline dripwaters has been shown to be almost exclusively complexed and transported by nano-scale organic colloids (Hartland et al., 2011, 2012).

It is interesting to compare the organic carbon content of stalagmites from different settings (Table 1). The removal efficiency of organic carbon in PC-08-1 appears to be high (ca. 3%) and it is clear that this is indeed a relatively high number, given that the TOC composition of PC-08-1 is substantially higher than in other stalagmites measured (Table 1). In addition, if the relationship in Eq. (9) is rearranged (Eq. (12)) we can estimate the free ion concentration

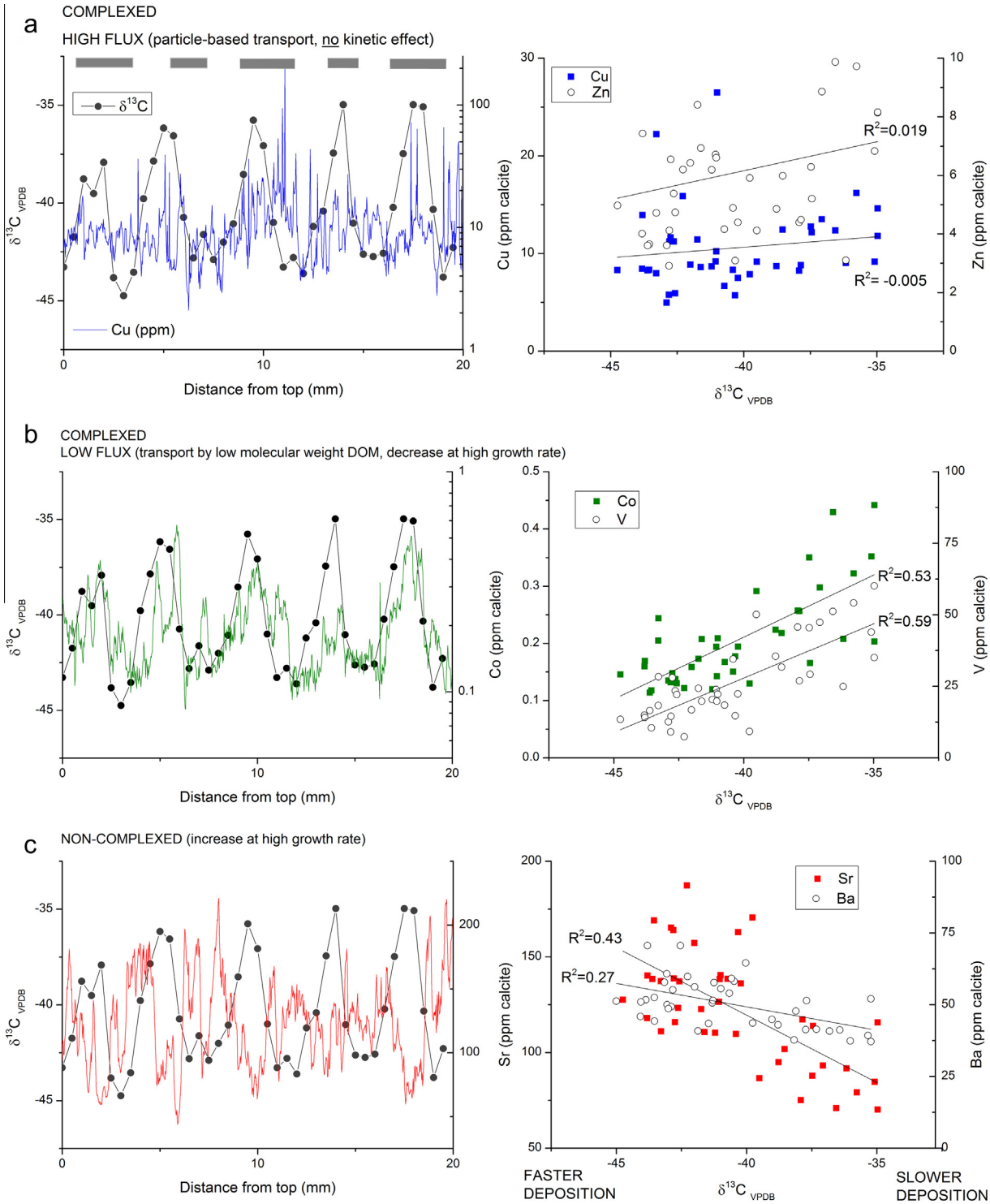

Fig. 8. Speleothem capture of NOM–metal complexes from dripwaters can be subdivided on the basis of the mode of transport (speciation in dripwaters) and the subsequent incorporation in the speleothem. Shaded boxes (a) indicate the approximate position of dark laminae in PC-08-1. For metals (Cu, Ni and Zn) carried by larger colloids (>100 nm) and particles (>1000 nm) (a; high-flux) the incorporation of the metal from the aqueous NOM–metal complex appears to occur independently of precipitation kinetics as indicated by $\delta^{13}C$ in this kinetically-disturbed system. For the metals (Co and V) carried by small colloids (1–100 nm) and nominally-dissolved NOM (<1 nm) (b) a kinetic effect is evident, with depletion occurring at high precipitation rates (lower $\delta^{13}C$). This is compared to the alkaline earth metals (c; Sr and Ba) which increase at higher precipitation rates (higher $\delta^{13}C$) because the discrimination between ions becomes less pronounced. Note that correlation between Co and Sr was not observed in dripwaters. The pattern of Co peaks seen in the stalagmite very closely corresponds to the fluorescence banding in stalagmite PC-97-1 described by (Baker et al., 1999b) further supporting the interpretation that Co directly corresponds to changes in the co-precipitation of NOM in calcite.

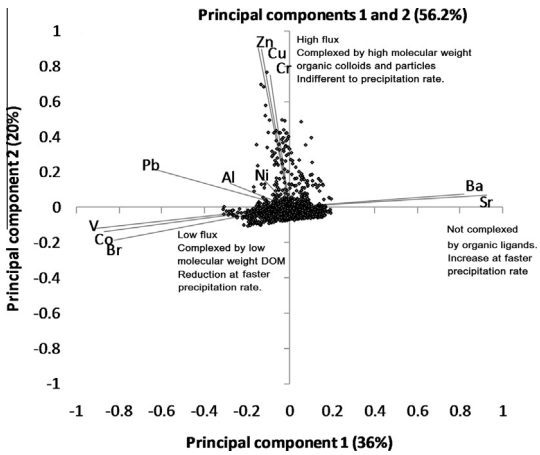

Fig. 9. Principal components analysis of average trace metal LA-ICPMS data acquired from two parallel traverses of the PC-08-1 stalagmite (see text for details).

in other cave waters, to see if we obtain reasonable values. In order to do this, an appropriate experimental inorganic K_d value for karst analogue conditions must be adopted.

$$f_{m(aq)} = \frac{\frac{M^{2+}(s)}{Ca^{2+}(s)} \cdot Ca^{2+}(aq)}{K_d} M^{2+}{}_{(aq)} \quad (12)$$

For example, if a value of 2.5 is used for Cu, the indicative free Cu fraction in Lower Balls Green Mine (LBGM) dripwaters is 0.53 – which is within the range of reasonable free metal fractions for Cu(II) in the presence of humic-like colloids, but certainly lower than the value predicted by equilibrium speciation codes of around 90–100% for LBGM dripwaters (Hartland et al., 2012). Clearly, inorganic K_d values for partitioning of transition metals into calcite under karst analogue conditions are needed to further test this hypothesis. It is important to note that a result of 0.53 for Cu only indicates the fraction of 'available' metal, i.e. free (hydrated) metal ions, plus that fraction of NOM–M which is able to dissociate in response to depletion of $Cu^{2+}{}_{(aq)}$ following adsorption on calcite. More data on trace metal lability at ca. pH 8 and relevant K_d values should allow the capture of NOM–M be clarified for all cave speleothems, enabling dripwater NOM–M fluxes to speleothems to be reconstructed.

3.5. Preservation of colloid-metal signals in hyperalkaline speleothem

Following the analysis of the partitioning of NOM–M complexes from dripwater into hyperalkaline speleothem PC-08-1, the next step is to see how seasonal changes in precipitation rate affect the capture of NOM–M from dripwaters. Since the most prominent feature of hyperalkaline carbonates is their prodigious vertical extension rates (0.1–2.5 cm yr^{-1}; Hartland et al., 2010b) they provide an ideal test of the effect of calcite precipitation rate on NOM–M incorporation and effects on other trace species.

High-resolution analysis of PC-08-1 by LA-ICPMS revealed distinct variations in trace metals. In Fig. 8, these contrasting trace metal signals are summarised showing elements that are representative of each class of behaviour in relation to the $\delta^{13}C_{VPDB}$ value in the corresponding layers. These encapsulate the high-flux metals (Fig. 8a; Cu, Zn, Ni), low-flux metals (Fig. 8b; Co, V) and alkaline earth metals (Fig. 8c; Sr, Ba).

The Co and Sr concentrations in PC-08-1 pale and dark laminae were negatively correlated in the sample ($R^2 = -0.57$, $n = 1439$) but was not correlated ($R^2 = 0.19$, $n = 21$) in dripwaters. When shown relative to $\delta^{13}C$, both Co and Sr show clear effects of precipitation rate variations on incorporation, since carbon isotopes are strongly kinetically fractionated in the sample (Fig. 3). Thus, this clear inverse relationship between Co (complexed by the finest nano-scale organic ligands) and Sr (not complexed) (Hartland et al., 2011) demonstrates that NOM is preferentially incorporated at low precipitation rates, and Sr is preferentially incorporated at high precipitation rates. Thus, these data imply that kinetics explain at least a component of the observed antipathy between transition metals (complexed by NOM) and the alkaline

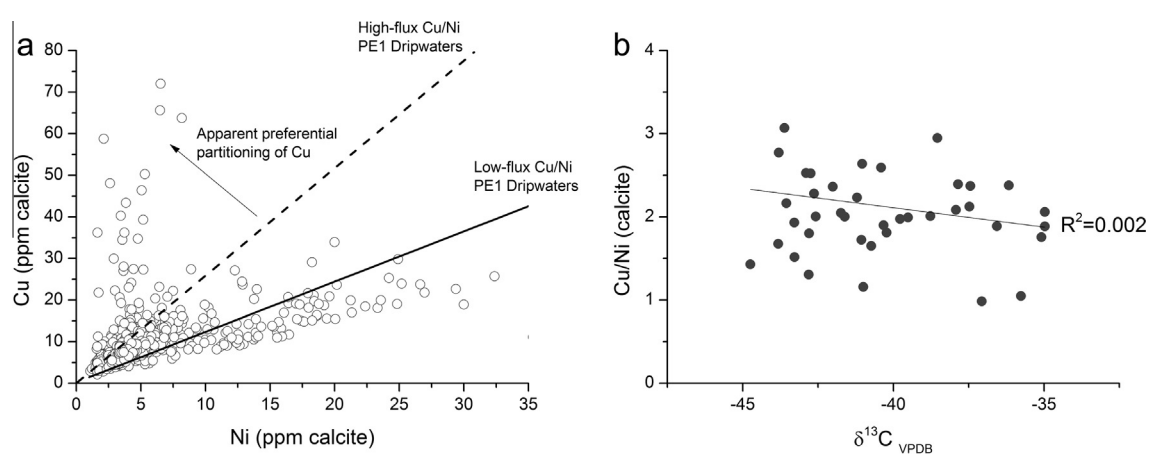

Fig. 10. LA-ICPMS data from PC-08-1 stalagmite showing the high-flux metals Cu and Ni relative to the corresponding trends measured in dripwaters. The preferential partitioning of Cu from the high-flux end-member (a) is shown to occur independently of calcite precipitation rate variations (b) as recorded by changes in carbon isotope ratios ($\delta^{13}C$).

earth metals in speleothems characterised by annual fluorescent laminae (with which these variations coincide spatially) (Borsato et al., 2007; Fairchild et al., 2010). In contrast to the antipathy in low-flux metals and the alkaline earth metals, the high-flux metals were clearly indifferent to precipitation rate variations (Fig. 8a), showing little evidence of seasonality, consistent with the more rapid, event-by-event delivery of these metals following infiltration in surface environments (Hartland et al., 2012). The distinctive behaviour of the various elements in PC-08-1 is exemplified in Fig. 9.

The association between trace elements was investigated using principal components analysis (Fig. 9). The principal component (PC1) explains 36% of the variability and separates the 'low-flux' metals (Co and V) and Br from the alkaline earth metals (Sr and Ba); PC2 explains 20% of the data and separates the 'high-flux' metals (Cu, Zn, Ni) as well as Cr, from the low-flux metals (Co and V) (Fig. 9). This analysis shows that trace elements in PC-08-1 may be sub-divided into three classes based on the results of dripwater monitoring studies: 'low-flux' (Co, V), 'high-flux' (Cu, Zn) and the alkaline earth metals (Sr and Ba); with the low-flux metals and the alkaline earth metals (Sr and Ba) showing strong negative correlation (Fig. 9).

Dripwater monitoring has identified prominent trends in trace metal ratios which show coherent changes following infiltration events in samples from Poole's Cavern, UK and Grotta d'Ernesto, Italy (Hartland et al., 2012). The trace metal data from LA-ICPMS scans of PC-08-1 reveals corresponding trends in the stalagmite, indicating the capture of the putative high- and low-molecular weight trace metal end-members (Fig. 10a). This analysis demonstrates that Cu partitions preferentially from NOM–Cu into the speleothem compared to NOM–Ni (Fig. 10a). By comparing Cu/Ni to $\delta^{13}C$ in the same layers (Fig. 10b), it is clear that the preferential partitioning of Cu relates to its tendency to bind strongly with the calcite surface (Lee et al., 2005; Elzinga et al., 2006) and not due to precipitation rate fluctuations. However, it is not obvious why Cu complexed by relatively higher molecular weight NOM should partition more than Cu from low molecular weight NOM. This may be due to stronger Cu complexation by smaller, nano-scale NOM because of their higher charge-densities (Benedetti et al., 1996). It is unlikely that inhibition of ternary complex formation by larger, high molecular weight colloids occurred since Cu/Ni in the PC-08-1 stalagmite did not show a relationship to precipitation rate changes ($\delta^{13}C$) (Fig. 10b).

4. CONCLUSION

The complete ternary surface complexation of an NOM–M complex (≡S-NOM–M) corresponds to a situation where the metal–ligand ratio in solution matches that in the solid. Thus, where metals are totally complexed by an organic ligand (NOM) and captured in stoichiometric unity, the partition coefficient $K_{d\ \mathrm{NOM\text{–}M}}$ for NOM–metal surface complexes ≈1, as shown here for NOM–Co.

In hyperalkaline solution, aqueous complexes between transition metals and NOM may be more stable than at lower pH (e.g. pH 7–8) as indicated by much lower measurable per cent free metal concentrations at pH 11 (Hartland et al., 2011). Our results show that in hyperalkaline systems, dissociation of metals during surface complexation with calcite is minimised for the strongest complexes with fine colloidal or nominally-dissolved NOM, leading to the relation $f_{\mathrm{m(aq)}} = \frac{\frac{\mathrm{M(s)}}{\mathrm{Ca(s)}}\cdot \mathrm{Ca(aq)}}{K_d} M_{\mathrm{(aq)}}$, where the difference between the apparent and actual K_d values of transition metals can be largely explained by the free metal concentration in solution. This requires testing in pH 7–8 speleothem-forming dripwaters and calcite growth experiments under karst analogue conditions before this relation can be generalised further.

The results of this study indicate that the relationship between the organic composition of speleothems and their trace metal compositions may be largely explained by the capacity of particulate, colloidal and nominally-dissolved NOM–M complexes to dissociate in the context of the ongoing interfacial process at the growing speleothem surface.

Natural organic matter in cave dripwaters clearly extends a pervasive influence over the abundance of surface-reactive metals, linked to effective rainfall and mediated by processes in soils (colloid and particle release), epikarst and aquifer (flow routing), and crystal surface (partitioning). We suggest that the distinct seasonality in humid and temperate climates is reflected in the chemical, isotopic and optical compositions of speleothems with depletions in alkaline earth metals (precipitation rate decreases) and enrichments in transition metals (colloidal delivery) being explained by antipathy between soil flushing (i.e. in autumn) and ventilation (i.e. winter).

The data presented here indicate that NOM–metal complexes are captured by speleothems. Once complexation reactions between NOM and metals at ca. pH 8 are better characterised, and when data on inorganic metal partitioning into calcite under karst analogue conditions are available, we predict that the trace metal composition of speleothems will be widely interpretable in terms of their organic contents, providing a record of colloid-facilitated transport, NOM character and concentration.

ACKNOWLEDGEMENTS

We are grateful to the Natural Environment Research Council (NERC) for funding through grants NE/G009317/1 and NE/G004048/1 and for a PhD studentship to A.H. (NER/S/A/2007/14396). This work was also partially funded through an award to A.H. by the British Cave Research Association (BCRA). The authors gratefully acknowledge the support of the NERC Facility for Environmental Nanoscience Analysis and Characterization, University of Birmingham and its technical staff and Stephen Baker for ICPMS analysis. Thanks are also given to the Buxton Civic Association and Poole's Cavern staff members for their invaluable assistance in facilitating this research. Thanks also to John Gunn and Andy Baker for help in site selection and support during the initial stages of this research. We are also grateful to Christoph Spötl, Silvia Frisia and Andrea Borsato for access to samples analysed as part of this research.

APPENDIX A. SUPPLEMENTARY DATA

Supplementary data associated with this article can be found, in the online version, at http://dx.doi.org/10.1016/j.gca.2013.12.005.

REFERENCES

Aiken G. R., Hsu-Kim H. and Ryan J. N. (2011) Influence of dissolved organic matter on the environmental fate of metals, nanoparticles, and colloids. *Environ. Sci. Technol.* **45**, 3196–3201.

Baker A., Caseldine C. J., Gilmour M. A., Charman D., Proctor C. J., Hawkesworth C. J. and Phillips N. (1999a) Stalagmite luminescence and peat humification records of palaeomoisture for the last 2500 years. *Earth Planet. Sci. Lett.* **165**, 157–162.

Baker A., Proctor C. J. and Barnes W. L. (1999b) Variations in stalagmite luminescence laminae structure at Poole's Cavern, England, AD 1910–1996: calibration of a palaeoprecipitation proxy. *Holocene* **9**, 683–688.

Baker A., Smart P. L., Edwards R. L. and Richards D. A. (1993) Annual growth banding in a cave stalagmite. *Nature* **364**, 518–520.

Benedetti M. F., VanRiemsdijk W. H., Koopal L. K., Kinniburgh D. G., Gooddy D. C. and Milne C. J. (1996) Metal ion binding by natural organic matter: from the model to the field. *Geochim. Cosmochim. Acta* **60**, 2503–2513.

Borsato A., Frisia S., Fairchild I. J., Somogyi A. and Susini J. (2007) Trace element distribution in annual stalagmite laminae mapped by micrometer-resolution X-ray fluorescence. Implications for incorporation of environmentally significant species. *Geochim. Cosmochim. Acta* **71**, 1494–1512.

Busenberg E. and Plummer L. N. (1985) Kinetic and thermodynamic factors controlling the distrubution of SO_4(2-) and Na^+ in calcites and selected aragonites. *Geochim. Cosmochim. Acta* **49**, 713–725.

Chada V. G. R., Hausner D. B., Strongin D. R., Rouff A. A. and Reeder R. J. (2005) Divalent Cd and Pb uptake on calcite [10(1)over-bar4} cleavage faces: an XPS and AFM study. *J. Colloid Interface Sci.* **288**, 350–360.

Clark I. D., Fontes J. C. and Fritz P. (1992) Stable isotope disequilibria in travertine from high pH waters: laboratory investigations and field observations from Oman. *Geochim. Cosmochim. Acta* **56**, 2041–2050.

Elzinga E. J., Rouff A. A. and Reeder R. J. (2006) The long-term fate of Cu^{2+}, Zn^{2+}, and Pb^{2+} adsorption complexes at the calcite surface. An X-ray absorption spectroscopy study. *Geochim. Cosmochim. Acta* **70**, 2715–2725.

Fairchild I. J. and Baker A. (2012) *Speleothem Science: From Process to Past Environments*. Wiley-Blackwell.

Fairchild I. J., Baker A., Borsato A., Frisia S., Hinton R. W., McDermott F. and Tooth A. F. (2001) Annual to sub-annual resolution of multiple trace-element trends in speleothems. *J. Geol. Soc.* **158**, 831–841.

Fairchild I. J. and Hartland A. (2010) Trace element variations in stalagmites: controls by climate and by karst system processes. In *Ion Partitioning in Ambient Temperature Aqueous Systems: From Fundamentals to Applications in Climate Proxies and Environmental Geochemistry* (eds. H. Stoll and M. Prieto). European Mineralogical Union, Oviedo.

Fairchild I. J., Spotl C., Frisia S., Borsato A., Susini J., Wynn P. M., Cauzid J. and Eimf (2010) Petrology and geochemistry of annually laminated stalagmites from an Alpine cave (Obir, Austria): seasonal cave physiology. *Geol. Soc. London Spec. Publ.* **336**, 295–321.

Fairchild I. J. and Treble P. C. (2009) Trace elements in speleothems as recorders of environmental change. *Quatern. Sci. Rev.* **28**, 449–468.

Fein J. B. (2002) The effects of ternary surface complexes on the adsorption of metal cations and organic acids onto mineral surfaces. In *Water–Rock Interactions, Ore Deposits, and Environmental Geochemistry. A Tribute to David A. Crerar* (ed. S. A. Wood). The Geochemical Society, St. Louis, p. 462.

Frisia S., Fairchild I. J., Fohlmeister J., Miorandi R., Spotl C. and Borsato A. (2011) Carbon mass-balance modelling and carbon isotope exchange processes in dynamic caves. *Geochim. Cosmochim. Acta* **75**, 380–400.

Godelitsas A., Astilleros J. M., Hallam K., Harissopoulos S. and Putnis A. (2003) Interaction of calcium carbonates with lead in aqueous solutions. *Environ. Sci. Technol.* **37**, 3351–3360.

Hartland A., Fairchild I. J., Lead J. R. and Baker A. (2010a) Fluorescent properties of organic carbon in cave dripwaters: effects of filtration, temperature and pH. *Sci. Total Environ.* **408**, 5940–5950.

Hartland A., Fairchild I. J., Lead J. R., Borsato A., Baker A., Frisia S. and Baalousha M. (2012) From soil to cave: transport of trace metals by natural organic matter in karst dripwaters. *Chem. Geol.* **304–305**, 68–82.

Hartland A., Fairchild I. J., Lead J. R., Dominguez-Villar D., Baker A., Gunn J., Baalousha M. and Ju-Nam Y. (2010b) The dripwaters and speleothems of Poole's Cavern: a review of recent and ongoing research. *Cave Karst Sci.* **36**, 37–46.

Hartland A., Fairchild I. J., Lead J. R., Zhang H. and Baalousha M. (2011) Size, speciation and lability of NOM-metal complexes in hyperalkaline cave dripwater. *Geochim. Cosmochim. Acta* **75**, 7533–7551.

Lead J. R. and Wilkinson K. J. (2006) Aquatic colloids and nanoparticles: current knowledge and future trends. *Environ. Chem.* **3**, 159–171.

Lee Y. J., Elzinga E. J. and Reeder R. J. (2005) Cu(II) adsorption at the calcite-water interface in the presence of natural organic matter: kinetic studies and molecular-scale characterization. *Geochim. Cosmochim. Acta* **69**, 49–61.

Longerich H. P., Jackson S. E. and Gunther D. (1996) Laser ablation inductively coupled plasma mass spectrometric transient signal data acquisition and analyte concentration calculation. *J. Anal. At. Spectrom.* **11**, 899–904.

Milne C. J., Kinniburgh D. G., Van Riemsdijk W. H. and Tipping E. (2003) Generic NICA-Donnan model parameters for metal-ion binding by humic substances. *Environ. Sci. Technol.* **37**, 958–971.

Murphy E. M., Zachara J. M., Smith S. C., Phillips J. L. (1990) The sorption of humic acids sorption of humic acids to mineral surfaces and their role in contaminant binding. In: *5th International Meeting of the International Humic Substances Soc: Advances in Humic Substances Research*, Nagoya, Japan. pp. 413–423.

Sunagawa I. (2005). In *Crystals. Growth, Morphology and Perfection*. Cambridge University Press.

Zachara J. M., Cowan C. E. and Resch C. T. (1991) Sorption of divalent metals on calcite. *Geochim. Cosmochim. Acta* **55**, 1549–1562.

Associate editor: Brian W. Stewart